JACS
JOURNAL OF THE AMERICAN CHEMICAL SOCIETY

Article

pubs.acs.org/JACS

Synthetic Supercontainers Exhibit Distinct Solution versus Solid State Guest-Binding Behavior

Feng-Rong Dai, Uma Sambasivam, Alex J. Hammerstrom, and Zhenqiang Wang*

Department of Chemistry, The University of South Dakota, Churchill-Haines Laboratories, Room 115, 414 East Clark Street, Vermillion, South Dakota 57069-2390, United States

Supporting Information

ABSTRACT: The phase-dependent host–guest binding behavior of a new family of synthetic supercontainers has been probed in homogeneous solution and at liquid–liquid, solid–liquid, and solid–gas interfaces. The synthetic hosts, namely, type II metal–organic supercontainers (MOSCs), are constructed from the assembly of divalent metal ions, 1,4-benzenedicarboxylate (BDC) linker, and sulfonylcalix[4]arene-based container precursors. One member of the MOSCs, MOSC-II-tBu-Ni, which is derived from Ni(II), BDC, and *p-tert*-butylsulfonylcalix[4]arene (TBSC), crystallizes in the space group $R\bar{3}$ and adopts pseudo face-centered cubic (fcc) packing, whereas other MOSCs, including TBSC analogue MOSC-II-tBu-Co, *p-tert*-pentylsulfonylcalix-[4]arene (TPSC) analogues MOSC-II-tPen-Ni/Co, and *p-tert*-octylsulfonylcalix[4]arene (TOSC) analogues MOSC-II-tOc-Ni/Mg/Co, all crystallize in the space group $I4/m$ and assume a pseudo body-centered cubic (bcc) packing mode. This solid-state structural diversity is nevertheless not reflected in their solution host–guest chemistry, as evidenced by the similar binding properties of MOSC-II-tBu-Ni and MOSC-II-tBu-Co in solution. Both MOSCs show comparable binding constants and adsorb ca. 7 equiv of methylene blue (MB) and ca. 30 equiv of aspirin in chloroform. In contrast, the guest-binding behavior of the MOSCs in solid state reveals much more variations. At the solid–liquid interface, MOSC-II-tBu-Co adsorb ca. 5 equiv of MB from an aqueous solution at a substantially faster rate than MOSC-II-tBu-Ni does. However, at the solid–gas interface, MOSC-II-tBu-Ni has higher gas uptake than MOSC-II-tBu-Co, contradicting their overall porosity inferred from the crystal structures. This discrepancy is attributed to the partial collapse of the solid-state packing of the MOSCs upon solvent evacuation. It is postulated that the degree of porosity collapse correlates with the molecular size of the MOSCs, i.e., the larger the MOSCs, the more severe they suffer from the loss of porosity. The same principle can rationalize the negligible N_2 and O_2 adsorption seen in the larger MOSC-II-tPen-Co and MOSC-II-tOC-Ni/Mg/Co molecules. MOSC-II-tPen-Ni features an intermediate molecular size and endures a partial structural collapse in such a way that the resulting pore dimension permits the inclusion of kinetically smaller O_2 (3.46 Å) but excludes larger N_2 (3.64 Å), explaining the observed remarkable O_2/N_2 adsorption selectivity.

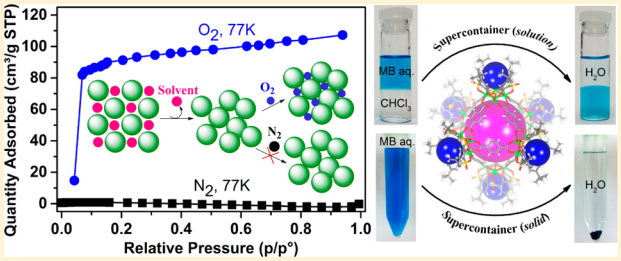

INTRODUCTION

Compartmentalization is a powerful strategy for both biological and synthetic systems to access confined space and controlled function.[1] Molecular containers, i.e., molecules containing convergent binding sites, are among those most widely studied in the context of host–guest chemistry.[2,3] Synthetic tools based on covalent,[4−13] coordination,[14−34] and hydrogen-bonding[35−42] linkages have afforded a diverse range of container structures. Coordination containers are particularly attractive thanks in part to the highly directional and relatively rigid nature of metal–ligand bonds.[43] The structural robustness of coordination containers renders them relevant in both solution and solid state, giving rise to various applications such as gas storage,[44−47] separation,[48,49] anion binding,[28,50−53] disaccharide recognition,[54,55] catalysis,[56−63] and drug delivery.[64−66] Compared to extended porous compounds such as metal–organic frameworks (MOFs),[67] coordination containers are advantageous for several of their molecular attributes including solution processability.[8,68−70]

A critical task in designing complex functions in container molecules is to fully understand their guest-binding behavior.[71] While this has been achieved in many synthetic containers, it is often separately done in solution[16,18,36] or in solid state,[72] despite the advantages of understanding the correlation between both interfaces.[73,74] One notable exception is the work demonstrated by Fujita and co-workers, who showed that the solution host–guest chemistry of their coordination containers can be reliably transferred into the solid state through ingenious design of "networked molecular cages".[73−75] Similarly, Cooper et al. discovered that the adsorption selectivity of a number of imine-based covalent containers in crystalline solids mirrored their guest-binding behavior in solution as a result of the intrinsic porous properties of these molecular organic cages.[76] Cooper's pioneering work further underscores the unique opportunities of utilizing molecular

Received: March 24, 2014
Published: May 1, 2014

Scheme 1. Assembly of Type II Metal–Organic Supercontainers

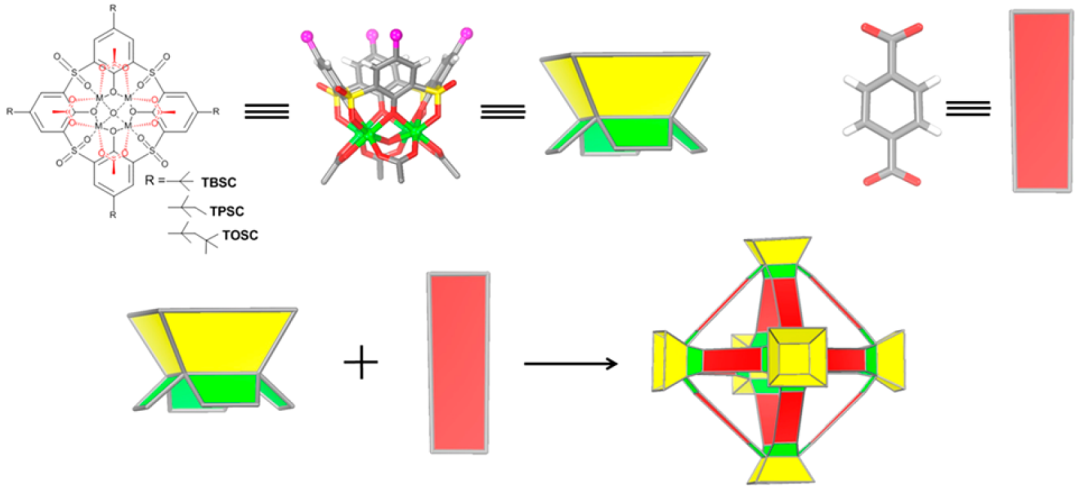

containers for designing new porous functions, as in principle it is possible to simultaneously modulate both "intrinsic" and "extrinsic" porosity,[77,78] which to date remains generally elusive.[79]

Recently, we showed that a family of prototypical (type I) octahedron-shaped coordination containers, namely, metal–organic supercontainers (MOSCs), can be constructed from the assembly of divalent metal ions [e.g., Ni(II), Mg(II), and Co(II)], sulfonylcalix[4]arenes,[80−82] and trigonal carboxylates (e.g., 1,3,5-benzenetricarboxylate, BTC) in a highly modular and predictable fashion.[83] These MOSCs were derived from the unusual linking of calixarenes[84] (i.e., at the lower rim) and distinguished by the presence of both *endo* and *exo* cavities.[85] Related compounds based on thiacalix[4]arenes were also recently reported by the laboratories of Liao[32] and Hong.[86] Following our initial report, we decided to examine the guest-binding behavior of these intriguing MOSC structures, with a specific aim to bridge the general knowledge gap between solution and solid-state properties of container molecules. We chose a new prototype of structures, namely, type II MOSCs, for this study owing to their robust synthesis and versatile solution and solid-state chemistry.

Type II MOSCs can be readily assembled from divalent metal ions, sulfonylcalix[4]arenes, and linear 1,4-benzenedicarboxylate (BDC) linker (Scheme 1). We show that these new members of MOSCs are ideally suited for pore engineering and that their intrinsic and extrinsic porosity can be tailored by modification of all three components, which has a subtle but distinct influence on their solution and solid-state properties. By replacing trigonal BTC with linear BDC, the pore volume and window size of the *endo* cavity of type II MOSCs are significantly expanded, without affecting the overall octahedral shape. Modification of metal ions from Co(II) to Ni(II) leads to an almost identical container structure and similar solution binding behavior with small molecules (e.g., an organic dye and a drug molecule) but results in a profound change in crystal packing and solid-state adsorption properties (i.e., extrinsic porosity). We further reveal that substituting *p-tert*-butylsulfonylcalix[4]arene (TBSC) with *p-tert*-pentylsulfonylcalix[4]arene (TPSC) or *p-tert*-octylsulfonylcalix[4]arene (TOSC) imparts intriguing O_2/N_2 adsorption selectivity to the MOSCs at the solid–gas interface but has a negligible effect in the solution. Our work thus represents the first systematic study that confirms container molecules may indeed exhibit phase-dependent guest-binding behavior. Identifying and understanding this phenomena will provide important guidelines for designing task-specific functions in porous materials, such as *capacity*-oriented storage applications vs *selectivity*-oriented separation applications.

EXPERIMENTAL DETAILS

General Methods. Unless otherwise noted, starting materials and solvents were obtained from commercial suppliers (Fisher Scientific, TCI, Alfa Aesar, Cambridge Isotope Laboratories, Inc., etc.) and used without further purification. ^{1}H NMR spectra were recorded on a Bruker Avance III HD NMR spectrometer (400 MHz), and the data were analyzed with the Topspin 3.2 software. The ultraviolet–visible (UV–vis) spectra were collected on a Varian Cary 5000 or Cary 50 UV–vis-NIR spectrophotometer. Thermogravimetric analysis (TGA) was performed at a scan speed of 2 °C/min under a stream of nitrogen on a TA Instruments Q600 SDT. Typical sample size ranged from ∼5 to 10 mg.

Synthesis. H_4TBSC, and H_4TOSC were synthesized as described in the literature.[80,82,87,88]

***p-tert*-Pentylthiacalix[4]arene.** The mixture of *p-tert*-pentylphenol (14.12 g, 0.086 mol), elemental sulfur S_8 (5.5 g, 0.172 mol), and NaOH (1.77 g, 0.043 mol) in tetraethylene glycol dimethyl ether (3.8 mL) was stirred under a nitrogen atmosphere. The mixture was gradually heated to 230 °C over a period of 4 h and then kept at this temperature for another 3 h with the removal of hydrogen sulfide. The resulting dark red product was cooled to room temperature and treated with 14 mL of toluene and 30 mL of H_2SO_4 (4 M) with stirring. After phase separation, methanol was added to the toluene phase to precipitate out the crude product. The resulting solid was collected by filtration, washed with acetone, and dried under vacuum with heating. Yield: 8.0 g (47.8%). ^{1}H NMR (400 MHz, $CDCl_3$): δ = 9.62 (s, 4H), 7.57 (s, 8H), 1.54 (q, J = 6.56 Hz, 8H), 1.17 (s, 24H), 0.64 (t, J = 6.83 Hz, 12H) ppm.

***p-tert*-Pentylsulfonylcalix[4]arene.** To a solution of *p-tert*-pentylthiacalix[4]arene (1.0 g, 1.28 mmol) in $CHCl_3$ (30 mL) were added acetic acid (50 mL) and $NaBO_3{\cdot}4H_2O$ (2.0 g, 13 mmol). The mixture was stirred at 50 °C for 18 h. Upon cooling, 30 mL of H_2O was added. The reaction product was then extracted with chloroform (30 mL × 3). After a drying step with $MgSO_4$, the chloroform solution was evaporated to dryness to give rise to the crude product. The crude solid was washed with acetone to afford an off-white product of *p-tert*-pentylsulfonylcalix[4]arene (1.05 g, 90.6%). ^{1}H NMR (400 MHz, d_6-DMSO): δ = 8.32 (s, 8H) 1.54 (q, J = 6.30 Hz, 8H), 1.21 (s, 24H), 0.54 (t, J = 6.24 Hz, 12H) ppm.

MOSC-II-tBu-Co. H_4TBSC (84.9 mg, 0.10 mmol), $Co(NO_3)_2{\cdot}6H_2O$ (145 mg, 0.50 mmol), and H_2BDC (54.8 mg, 0.33 mmol) were

dx.doi.org/10.1021/ja502839b | J. Am. Chem. Soc. 2014, 136, 7480−7491

dissolved in 10 mL of *N*,*N*-dimethylformamide (DMF) in a scintillation vial (20 mL capacity). The vial was then transferred to a programmable oven and heated at a rate of 0.5 °C/min from 35 to 100 °C. The temperature was held at 100 °C for 24 h before cooling to 35 °C at a rate of 0.2 °C/min. This procedure resulted in a clear dark red solution, which was then divided into 3 vials and placed in a jar containing diethyl ether (or ethyl acetate) for solvent slow diffusion. Pink crystals of MOSC-II-tBu-Co formed after 2 d, and were isolated by washing with diethyl ether and dried in the air to afford 82 mg of the as-synthesized material.

MOSC-II-tBu-Ni. H_4TBSC (84.9 mg, 0.10 mmol), $Ni(NO_3)_2{\cdot}6H_2O$ (145 mg, 0.50 mmol), and H_2BDC (54.8 mg, 0.33 mmol) were dissolved in 10 mL of DMF in a scintillation vial (20 mL capacity). The vial was then transferred to a programmable oven and heated at a rate of 0.5 °C/min from 35 to 100 °C. The temperature was held at 100 °C for 24 h before cooling to 35 °C at a rate of 0.2 °C/min. This procedure resulted in a clear brownish yellow solution, which was then divided into 3 vials and placed in a jar containing ethyl acetate (or diethyl ether) for solvent slow diffusion. After 3 d, green crystals of MOSC-II-tBu-Ni were obtained and isolated to afford 65 mg of the as-synthesized material.

MOSC-II-tPen-Co. H_4TPSC (9.05 mg, 0.010 mmol), $Co(NO_3)_2{\cdot}6H_2O$ (14.5 mg, 0.05 mmol), and H_2BDC (5.5 mg, 0.033 mmol) were dissolved in DMF (0.7 mL) in a dram vial (4 mL capacity). The vial was then transferred to a programmable oven and heated at a rate of 0.5 °C/min from 35 to 100 °C. The temperature was held at 100 °C for 24 h before cooling to 35 °C at a rate of 0.2 °C/min. This procedure resulted in a clear dark red solution, which was placed in a jar containing ethyl acetate (or diethyl ethyl) for solvent slow diffusion. After 3 days, pink crystals were obtained to afford 4 mg of the as-synthesized material.

MOSC-II-tPen-Ni. H_4TPSC (90.5 mg, 0.10 mmol), $NiCl_2{\cdot}6H_2O$ (118 mg, 0.5 mmol), and H_2BDC (54.8 mg, 0.33 mmol) were dissolved in DMF (5 mL) in a scintillation vial (20 mL capacity). The vial was then transferred to a programmable oven and heated at a rate of 0.5 °C/min from 35 to 100 °C. The temperature was held at 100 °C for 24 h before cooling to 35 °C at a rate of 0.2 °C/min. This procedure resulted in a clear green solution. Then, 3 mL of methanol solution was added, and the vial was transferred to a programmable oven and reheated at a rate of 0.5 °C/min from 35 to 75 °C. The temperature was held at 75 °C for 3 h before cooling to 35 °C at a rate of 0.1 °C/min. Green crystals were isolated by washing with MeOH and dried in the air to afford 43 mg of the as-synthesized material.

MOSC-II-tOc-Co. H_4TOSC (107.5 mg, 0.10 mmol), $Co(NO_3)_2{\cdot}6H_2O$ (145.8 mg, 0.50 mmol), and H_2BDC (36.5 mg, 0.22 mmol) were dissolved in DMF (10 mL) in a scintillation vial (20 mL capacity). The vial was then transferred to a programmable oven and heated at a rate of 0.5 °C/min from 35 to 100 °C. The temperature was held at 100 °C for 24 h before cooling to 35 °C at a rate of 0.2 °C/min. Pink crystals of MOSC-II-tOc-Co were isolated by washing with MeOH and dried in the air to afford 120 mg of the as-synthesized material.

MOSC-II-tOc-Ni. H_4TOSC (53.7 mg, 0.050 mmol), $Ni(NO_3)_2{\cdot}6H_2O$ (72.7 mg, 0.25 mmol), and H_2BDC (27.8 mg, 0.167 mmol) were dissolved in a mixture solvent of DMF (10 mL) and MeOH (5 mL) in a scintillation vial (20 mL capacity). The vial was then transferred to a programmable oven and heated at a rate of 0.5 °C/min from 35 to 100 °C. The temperature was held at 100 °C for 24 h before cooling to 35 °C at a rate of 0.2 °C/min. Green crystals of MOSC-II-tOc-Ni were isolated by washing with MeOH and dried in the air to afford 71 mg of the as-synthesized material.

MOSC-II-tOc-Mg. H_4TOSC (53.7 mg, 0.05 mmol), $Mg(NO_3)_2{\cdot}6H_2O$ (64.1 mg, 0.25 mmol), and H_2BDC (27.7 mg, 0.167 mmol) were dissolved in a mixture solvent of DMF (10 mL) and MeOH (5 mL) in a scintillation vial (20 mL capacity). The vial was then transferred to a programmable oven and heated at a rate of 0.5 °C/min from 35 to 100 °C. The temperature was held at 100 °C for 24 h before cooling to 35 °C at a rate of 0.2 °C/min. Colorless crystals of MOSC-II-tOc-Mg were isolated by washing with MeOH and dried in the air to afford 65 mg of the as-synthesized material.

X-ray Crystallography. X-ray single-crystal diffraction data were collected at 100 K using graphite-monochromated Mo Kα radiation (λ = 0.71073 Å) on a Bruker CCD APEXII diffractometer. The collected frames were processed with the software SAINT. The data were corrected for absorption by using the SADABS program. The structure was solved by the Direct methods (SHELX97) in conjunction with standard difference Fourier techniques and subsequently refined by full-matrix least-squares analyses on F^2. Hydrogen atoms were generated in their idealized positions, and all non-hydrogen atoms were refined anisotropically. The electron count due to disordered solvent in the void space of the crystals was calculated using the program SQUEEZE in PLATON software package.

Host–Guest Binding Experiments. The solution and solid-state guest-binding behavior of type II MOSCs was probed at four different platforms, i.e., homogeneous solution, liquid–liquid, solid–liquid, and solid–gas interfaces.

Homogeneous-Solution Guest Binding. The solution host–guest chemistry was probed using the UV–vis titration technique.[89] Stock solutions of the MOSCs were prepared in $CHCl_3$ at a concentration of ~5×10^{-6} M. Then, 25.00 mL of the stock solution was used to dissolve an accurately known mass of methylene blue (MB) or aspirin, chosen to yield a solution at a concentration 20–100 times greater than that of the MOSC. Subsequently, 2.00 mL of the MOSC solution was placed in a 10.0 mm quartz cell, upon which 0.01–2 mL of the MB or aspirin solution was added gradually. After each addition, the cell was stoppered and inverted, and the UV–vis spectrum was collected (at 25 °C) after 5 min to ensure complete mixing and reaching equilibration.

To evaluate the overall binding strength, the titration results were fitted to the linear form of Benesi–Hildebrand (B–H) equation:[90]

$$\frac{1}{\Delta A} = \frac{1}{l\Delta\varepsilon[G]_0[H]_0K_a} + \frac{1}{l\Delta\varepsilon[H]_0}$$

where ΔA (= $A_{obs} - A_0$) is the change in absorbance, l (= 1 cm) is the path length, $\Delta\varepsilon$ (= $\varepsilon^{HG} - \varepsilon^{H}$) is the difference in extinction coefficient between host–guest complex and free MOSC, $[G]_0$ is initial guest concentration, $[H]_0$ is the initial MOSC concentration, and K_a is the association constant.

Liquid–Liquid Extraction. Aqueous stock solutions of MB were prepared by dissolving the dye in deionized water. Five milliliters of the aqueous dye solution ($3 \times 10^{-5} \sim 1.3 \times 10^{-4}$ M) was then added to 5 mL of chloroform solution containing the MOSC ($4 \times 10^{-6} \sim 1.2 \times 10^{-5}$ M). The mixture was shaken for 1 min and kept in dark at room temperature for 4 h prior to UV–vis measurements, allowing the aqueous and chloroform layers to fully separate. Control experiments were set up in a similar manner except that the MOSC solutions were replaced by straight chloroform solvents. The UV–vis spectra of the aqueous and chloroform phases were recorded on a spectrophotometer. The remaining concentration of MB in the aqueous phase was directly determined on the basis of the absorbance at 664 nm using a previously determined calibration curve. The concentration of MB in the chloroform phase was calculated by subtracting the remaining dye concentration in the aqueous solution from the dye concentration of the aqueous stock solution.

Solid–Liquid Adsorption. The MOSCs were dried on a Schlenk line at 120 °C for 10 h prior to use. An aqueous stock solution of MB was prepared by dissolving MB in deionized water. A precisely weighted amount of the MOSCs (~4 mg) was placed in a diluted MB solution (100 mL) and the suspension was fully mixed with stirring at room temperature. The concentrations of the MB solutions were determined on the basis of the absorbance at 664 nm using a calibration curve. The UV–vis spectra of the solutions were monitored at different time intervals to determine the concentration of the remaining (i.e., unadsorbed) MB.

Time-dependent adsorption of MB by MOSCs is treated with the pseudo-second-order kinetic model:[91]

$$\frac{t}{q_t} = \frac{1}{k_2 q_e^2} + \frac{1}{q_e}t$$

where q_e and q_t are the sorption capacity (mol/mol) at equilibrium and at time t, respectively, and k_2 is the rate constant. The pseudo-second-order kinetic constant (k_2) can be calculated via k_2 = slope^2/intercept when t/q_t is plotted against t.

Solid−Gas Adsorption. Gas adsorption isotherms were measured using a Micromeritics ASAP2020 instrument based on a volumetric method. Samples were typically predried on a Schlenk line at 120 °C for 5 h to overnight before they were transferred to preweighed analysis tubes, which were then capped with seal frits. Activation method based on solvent exchange was found to have little impact on the gas adsorption results (Figure S34). The samples were degassed under dynamic vacuum (<6 μmHg) at 105 °C for ∼24−48 h until the outgas rates were lower than 5 μmHg/min. The analysis tubes containing the evacuated samples were weighed again to determine the sample weights (typically ∼100 mg for most samples) before they were transferred back to the analysis port of the instrument. The N_2 and O_2 isotherms were measured at 77 K in a liquid N_2 bath using ultra high pure (UHP) grade N_2 or O_2 gases (99.99%). The CO_2 isotherms were measured at 196 K in a dry ice/2-propanol bath using UHP grade CO_2 gas (99.99%).

RESULTS AND DISCUSSION

Synthesis and Structure. Sulfonylcalixarenes, sulfur analogues of calixarenes,[84] represent an important subset of macrocyclic containers that are composed of phenolic units linked by sulfonyl groups.[80−82] The coordination chemistry of sulfonylcalix[4]arenes with metal cations and acetate anions afforded an interesting class of tetranuclear complexes in which four phenoxo and four sulfonyl oxygen atoms coordinate to four metal ions that are in turn bound by one μ_4-oxygen and four acetate groups at the lower rim of the sulfonylcalix[4]-arenes (Scheme 1, top).[92] Type II MOSCs were readily obtained when acetate was replaced by the linear dicarboxylate linker BDC (Scheme 1, bottom). The reaction of cobalt(II) nitrate, H_4TBSC, and H_2BDC in DMF at 100 °C for 24 h, followed by vapor diffusion in diethyl ether or ethyl acetate for 48 h, afforded pink, block-shaped crystals. Single-crystal X-ray diffraction (XRD) study revealed that the compound, designated as MOSC-II-tBu-Co, has an edge-directed octahedral container structure and is composed of six tetranuclear complex units bridged by 12 BDC ligands (Figure 1 and Figure S1). MOSC-II-tBu-Co can be formulated as $\{[Co_4(\mu_4\text{-}H_2O)(TBSC)]_6(BDC)_{12}\}\cdot(DMF)_x\cdot(H_2O)_y$ ($x \approx 70$; $y \approx 90$) based on the XRD, TGA, and elemental analysis results. It shares many structural features with the type I MOSC series,[83]

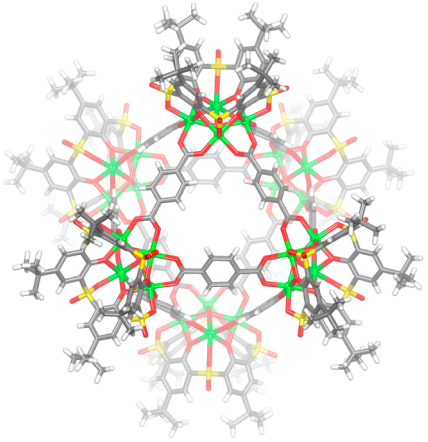

Figure 1. Crystal structure of MOSC-II-tBu-Co. Color scheme: Co, green; S, yellow; O, red; C, gray; H, white.

including a multipore (i.e., *endo* and *exo* cavities) architecture, C_{4h} molecular symmetry, and pseudo body-centered cubic (bcc) crystal packing (i.e., $I4/m$ space group; Figure 2, left).

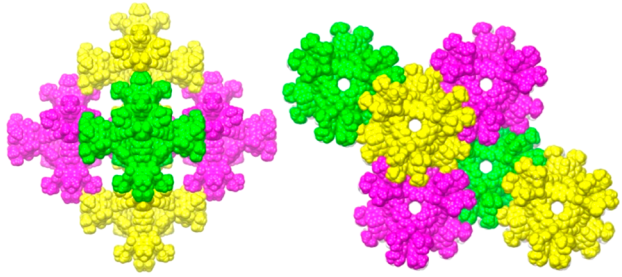

Figure 2. (Left) Pseudo body-centered cubic packing of MOSC-II-tBu-Co; (right) pseudo face-centered cubic packing of MOSC-II-tBu-Ni.

This latter feature similarly results in the formation of noncovalent octahedra by virtue of hydrophobic interactions between *tert*-butyl groups from six adjacent container molecules (Figure S8). However, compared to its type I counterparts, the *endo* cavity and window openings of MOSC-II-tBu-Co are significantly expanded. While its inner and outer diameters (ca. 1.7 and 3.3 nm, respectively) are only slightly longer than those of the corresponding type I MOSC (1.4 and 3.0 nm, respectively), its internal volume (ca. 1.2 nm^3; Figure S9) is estimated to be more than twice that of the latter (ca. 0.55 nm^3). Notably, MOSC-II-tBu-Co contains eight triangular windows that have a widest opening of ca. 6.5 Å (i.e., the distance between two opposing carboxylate oxygen atoms), which is considerably wider than the portal dimensions observed in the type I MOSC (ca. 1.0 Å x 2.3 Å). It may be expected that rotation of benzene rings in the BDC ligand[93] could lead to further opening of the windows.

The nickel(II) analogue, MOSC-II-tBu-Ni, can also be obtained as a single-crystalline product in a similar fashion. MOSC-II-tBu-Ni has an octahedral container framework very similar to the Co (II) compound (Figure S2). However, the structure of MOSC-II-tBu-Ni has strikingly distinct C_3 molecular symmetry, instead of the C_{4h} symmetry seen in MOSC-II-tBu-Co. This suggests that each individual molecule of MOSC-II-tBu-Ni is chiral, as it has no improper rotational symmetry. This surprising chirality can be attributed to the asymmetric arrangement of the achiral building blocks (Figure S10) and MOSC-II-tBu-Ni is thus reminiscent of the "snub cube" reported by MacGillivray and Atwood.[38] The molecular chirality of MOSC-II-tBu-Ni nevertheless does not translate into solid state and the container molecule crystallizes in the achiral space group $R\bar{3}$, indicating that the crystal contains a racemic mixture of both enantiomers. Unlike MOSC-II-tBu-Co, which adopts pseudo bcc packing, the crystal structure of MOSC-II-tBu-Ni assumes a pseudo face-centered cubic (fcc) packing mode (Figure 2, right). The most direct outcome of this structural distinction is the substantially different extrinsic porosity shown by the two crystalline phases. The crystal structure of MOSC-II-tBu-Co manifests open channels that are much wider in diameter owing to its non-close bcc packing, although the channels do not directly run through its triangular windows (Figure 2, left). In contrast, while MOSC-II-tBu-Ni has considerably narrower channels as a result of its pseudo-close fcc packing mode, the direction of the channels coincides

dx.doi.org/10.1021/ja502839b | J. Am. Chem. Soc. 2014, 136, 7480−7491

Table 1. Crystallographic Data for Type-II MOSCs

MOSC-II-	tBu-Ni	tBu-Co	tPen-Ni	tPen-Co	tOc-Ni	tOc-Mg	tOc-Co
Empirical formula	$C_{336}H_{324}Ni_{24}O_{126}S_{24}$	$C_{336}H_{324}Co_{24}O_{126}S_{24}$	$C_{360}H_{372}Ni_{24}O_{126}S_{24}$	$C_{360}H_{372}Co_{24}O_{126}S_{24}$	$C_{432}H_{516}Ni_{24}O_{126}S_{24}$	$C_{432}H_{516}Mg_{24}O_{126}S_{24}$	$C_{432}H_{516}Co_{24}O_{126}S_{24}$
Formula weight	8556.43	8561.71	8893.06	8898.34	9902.93	9077.33	9908.21
Temperature (K)	100	100	100	100	100	100	100
Crystal system	Rhombohedral	Tetragonal	Tetragonal	Tetragonal	Tetragonal	Tetragonal	Tetragonal
space group	$R\bar{3}$	$I4/m$	$I4/m$	$I4/m$	$I4/m$	$I4/m$	$I4/m$
a (Å)	40.715(2)	26.0148(12)	29.335(5)	29.335(6)	29.2376(18)	29.6397(16)	29.5252(14)
b (Å)	40.715(2)	26.0148(12)	29.335(5)	29.335(6)	29.2376(18)	29.6397(16)	29.5252(14)
c (Å)	80.041(8)	43.710(4)	41.486(2)	41.358(10)	42.213(5)	42.389(4)	42.576(4)
α (deg)	90	90	90	90	90	90	90
β (deg)	90	90	90	90	90	90	90
γ (deg)	120	90	90	90	90	90	90
V (Å^3)	114906(14)	33756(6)	35701(9)	35590(14)	36085(5)	37239(5)	37115(4)
Z	6	2	2	2	2	2	2
D(calcd) (g cm^{-3})	0.742	0.842	0.827	0.830	0.911	0.810	0.887
μ (Mo K$_\alpha$) (mm^{-1})	0.682	0.694	0.733	0.660	0.731	0.140	0.638
Reflections collected/unique	329649/44737 [R_{int} = 0.0852]	96887/9319 [R_{int} = 0.0765]	160406/14673 [R_{int} = 0.1146]	65844/10405 [R_{int} = 0.1375]	87017/6718 [R_{int} = 0.0611]	70187/5043 [R_{int} = 0.0535]	109385/8700 [R_{int} = 0.0647]
Data/restraints/parameters	44737/90/1552	9319/39/606	14673/24/643	10405/125/640	6718/277/727	5043/458/723	8700/313/712
GOF	1.032	1.590	1.042	1.121	1.538	1.095	1.236
R_1, wR_2 ($I > 2\sigma(I)$)	0.1564, 0.4164	0.1496, 0.3957	0.0957, 0.2529	0.1391, 0.3470	0.1074, 0.3241	0.1341, 0.4214	0.1010, 0.3149
R_1, wR_2 (all data)	0.2099, 0.4916	0.1709, 0.4310	0.1350, 0.2774	0.1917, 0.3755	0.1203, 0.3423	0.1425, 0.4411	0.1161, 0.3355

dx.doi.org/10.1021/ja502839b | J. Am. Chem. Soc. 2014, 136, 7480−7491

with its 3-fold rotational axis and triangular windows (Figure 2, right).

Interestingly, this metal-ion-dependent effect that directs crystal packing is not as clear when TBSC is replaced by its slightly bulkier analogues TPSC and TOSC (Scheme 1) in the assembly of type II MOSCs. Indeed, the two new Ni(II)-based MOSCs, MOSC-II-tPen-Ni and MOSC-II-tOc-Ni, do not show the same pseudo fcc packing as MOSC-II-tBu-Ni does; instead, they crystallize in the *I*4/*m* space group and adopt the pseudo bcc packing seen in MOSC-II-tBu-Co, MOSC-II-tPen-Co, and MOSC-II-tOc-Co (Table 1). Neither is this effect immediately apparent when type II MOSCs are constructed from other metal ions and a Mg (II) analogue, MOSC-II-tOc-Mg, is found to crystallize in the *I*4/*m* phase. On the basis of these observations, we propose that the two crystallographic phases arise as a result of the subtle difference in the molecular size of the MOSCs, i.e., smaller MOSCs favor the more close-packed fcc mode and larger MOSCs adopt the non-close-packed bcc mode. Both metal ion radii (and M−O distances) and upper-rim substitutions of sulfonylcalixarenes are expected to contribute directly to the molecular size of the MOSCs. The Shannon ionic radii for the three metal ions are in the order of Ni^{2+} (0.83 Å) < Mg^{2+} (0.86 Å) < Co^{2+} (0.89 Å),[94] and the corresponding average M−O bond distances in the seven MOSCs reported herein follow a similar trend: Ni(II)-O (2.069 Å) < Mg(II)-O (2.106 Å) < Co(II)-O (2.116 Å). On the other hand, sequentially incorporating *tert*-butyl, *tert*-pentyl, and *tert*-octyl substitutions leads to increasing molecular sizes of the MOSCs. We thus postulate that MOSC-II-tBu-Ni, combining the marginally smaller Ni (II) ions and *tert*-butyl groups, has a molecular size just small enough to adopt the fcc packing, whereas replacement with larger Co (II)/Mg (II) ions or bulkier *tert*-pentyl/*tert*-octyl groups leads to larger MOSCs favoring the bcc packing. Although full structural refinements are currently not available due to poor diffraction quality, preliminary single-crystal X-ray crystallographic analysis suggests that type II MOSCs based on Ni (II), TBSC, and 2-NH_2-BDC or 2-Br-BDC also crystallize in the $R\bar{3}$ space group and are isomorphic to MOSC-II-tBu-Ni (Table S2). This finding further supports our hypothesis, as examination of the type II MOSC structures (Figure 1) suggests that the bromo- and amino-substitutions on the BDC linker should not cause any significant change to the molecular size of the MOSCs.

Solution Host−Guest Binding. Solution processability is one of the most significant features of container molecules when compared to other types of nanoporous structures, as it provides a convenient handle for material fabrication and for probing host−guest chemistry. The seven type-II MOSCs are most soluble in chloroform, although the solubility is found to fluctuate, ranging from 10^{-6} to 10^{-3} M, often sensitive to the pretreatment of the MOSCs. Typically, evacuating the samples under vacuum for extended periods and at elevated temperatures (e.g., 100 °C) leads to substantially higher solubility for most compounds, indicating the importance of sample activation, which likely helps overcome the solid-state packing interactions and facilitates solvation of individual container molecules. It should be noted that the MOSCs are thermally stable up to 400 °C in solid state, as indicated by the TGA curves (Figures S12 and S13), and should therefore be robust enough to sustain the thermal treatment. The structural integrity of dissolved MOSCs in solution is also confirmed by NMR (Figure S14), UV−vis (Figure S15), and mass spectrometry (Figures S16 and S17; Table S3).

To understand the binding behavior of type II MOSCs in solution, two representative guests, namely, a dye molecule methylene blue (MB) and a drug molecule aspirin (Scheme 2),

Scheme 2. Structures of Two Guest Molecules

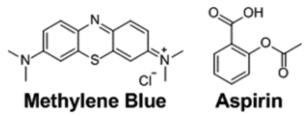

were chosen as molecular probes. These two guests were selected for their broad implications in dye encapsulation[95] and drug delivery,[96] respectively, as well as their suitable spectroscopic and solubility characteristics. Binding of the MOSCs with both guests in chloroform at ambient conditions was monitored by supramolecular UV−vis titration technique.[89] Taking MOSC-II-tBu-Co as an illustrative example, the MOSC has a maximum absorption band at 347 nm (Figure S15), whereas MB and aspirin have a maximum absorption band at 665 and 275 nm, respectively (MB has a second absorption band at 294 nm).

Binding of MOSC-II-tBu-Co with MB is clearly indicated by a red shift of the MOSC absorption maxima from 347 to 350 nm upon gradual increase of the guest equivalents (Figure 3, left). Fitting the titration data to the well-known Benesi−Hildebrand (B−H) equation[90] gives rise to an apparent association constant of $(1.42 \pm 0.31) \times 10^4$ M^{-1} (Figure 3, right; Table S5), indicating relatively robust overall binding between the MOSC and MB.[97] When subjected to the same UV−vis titration analysis, MOSC-II-tBu-Ni exhibits very similar behavior as MOSC-II-tBu-Co, featuring a red shift of the MOSC absorption maxima from 348 to 352 nm upon gradual increase of MB equivalents (Figure 3, middle) and an almost identical apparent association constant, $(1.24 \pm 0.32) \times 10^4$ M^{-1} (Figure 3, right; Table S6). This indicates that, in contrast to the subtle role they play in modulating crystal packing, the influence of metal ions is negligible in the liquid phase and the solution guest-binding propensity of MOSCs is essentially dictated by individual supercontainer structure.

To further quantify MB binding in solution, efforts were made to determine the binding stoichiometry. While linear B−H equation provides valuable insights into the host−guest binding, it does not specify binding stoichiometry and describes only overall effect averaging from the multiple, stepwise recognition processes expected for the MOSCs. Attempts to utilize Job's method of continuous variations[98] to determine the [MB]/[MOSC] ratio were nevertheless unsuccessful, likely because there exist more than one host−guest complex due to the multiple binding cavities of the MOSCs.[99] Plots of absorbance vs [MB]/[MOSC] ratio commonly used to determine guest stoichiometry (vide infra)[100] also did not yield useful information as a result of overlapping between the shoulder of the second MB absorption maxima (294 nm) and the MOSCs absorption maxima (~350 nm) at higher guest equivalents. To resolve this issue, we designed guest binding experiments at a liquid−liquid interface. The MOSC and MB were dissolved in two immiscible solvents, namely, chloroform and water, respectively. Since MB is predominantly more soluble in water, it dissolves almost exclusively in the aqueous phase at the H_2O−$CHCl_3$ interface in the absence of MOSC (Figure 4a, middle). However, in the presence of MOSC-II-tBu-Co, molecules of MB are quickly extracted into the $CHCl_3$

dx.doi.org/10.1021/ja502839b | J. Am. Chem. Soc. 2014, 136, 7480−7491

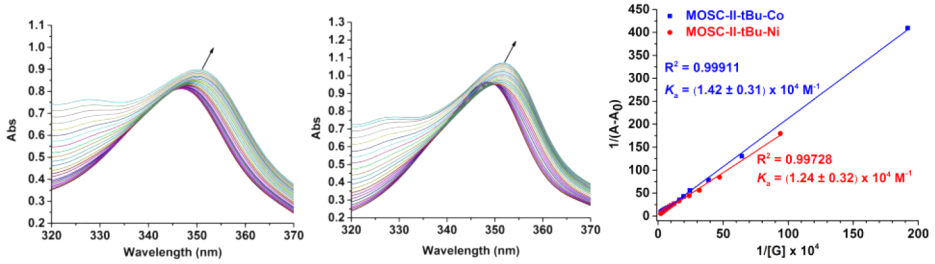

Figure 3. UV−vis spectra of MOSC-II-tBu-Co (left) and MOSC-II-tBu-Ni (middle) upon titration with methylene blue, and the linear fits to Benesi−Hildebrand equation (right). The arrows indicate gradual increase of methylene blue equivalents.

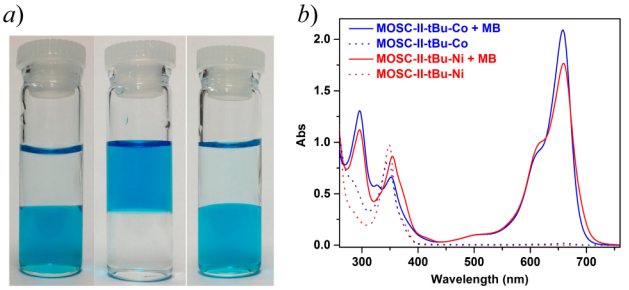

Figure 4. (a) H_2O−$CHCl_3$ extraction of methylene blue in the presence of MOSC-II-tBu-Co (left), absence of MOSC (middle), and presence of MOSC-II-tBu-Ni (right) in $CHCl_3$ phase (lower portions); (b) UV−vis spectra of MOSC-II-tBu-Co and MOSC-II-tBu-Ni in $CHCl_3$ phase before (dash lines) and after (solid lines) methylene blue extraction.

phase (Figure 4a, left). Such a drastic reverse of MB solubility is further confirmed by the UV−vis spectra of MOSC-II-tBu-Co in the $CHCl_3$ phase before and after the extraction (Figure 4b) and is a strong indication of the robust host−guest binding. The liquid−liquid platform also provides a unique opportunity for determining binding stoichiometry, since the majority of free MB molecules remain in the aqueous phase and bounded MB molecules can thus be indirectly quantified using UV−vis spectra obtained from the aqueous solution. Indeed, calculations based on the aqueous UV−vis spectra and calibration curves indicate a [MB]/[MOSC] ratio of 7.01 ± 0.08 for MOSC-II-tBu-Co (Table S4). A stoichiometric ratio of ∼7 is reasonable, as one may anticipate the MOSC binds to six MB molecules through its *exo* cavities (i.e., one MB molecule per cavity) and one MB molecule through its *endo* cavity. Therefore, the liquid−liquid extraction experiments not only highlight the potentials of MOSCs for separation applications, they also provide an effective tool to understand the solution chemistry of MOSCs.

When analogous liquid−liquid extraction experiments were carried out on the MOSC-II-tBu-Ni system, it was revealed to behave very similarly to its cobalt counterpart (Figure 4a, right and Figure 4b), manifesting a [MB]/[MOSC] binding ratio of 6.96 ± 0.19, almost identical to that of MOSC-II-tBu-Co (Table S4). In addition, it is found that substitution of *tert*-butyl groups with bulkier *tert*-pentyl or *tert*-octyl units does not lead to any significant change in the solution MB-binding properties of the MOSCs (Figures S18−S21; Table S7) These results again imply that the solution guest-binding behavior of type II MOSCs depends primarily upon individual container architecture.

Binding of the aspirin guest by the MOSCs was similarly probed using the protocols detailed above. When this is compared to the case of MB, a notable distinction of the aspirin binding is evidenced by the absence of any significant red shift in the UV−vis titration curves. Instead, only a gradual increase of the maximum absorption intensity of the MOSCs (at 347 nm for MOSC-II-tBu-Co and 348 nm for MOSC-II-tBu-Ni, respectively) is observed upon sequential addition of aspirin equivalents (Figures S22 and S23). The overall binding strength of aspirin with the MOSCs is weaker than that of MB with the MOSCs,[101] as is confirmed by the B−H analysis results, which give rise to an apparent association constant of (5.86 ± 0.50) × 10^3 and (6.34 ± 0.22) × 10^3 M^{-1} for MOSC-II-tBu-Co and MOSC-II-tBu-Ni, respectively (Figure 5). These

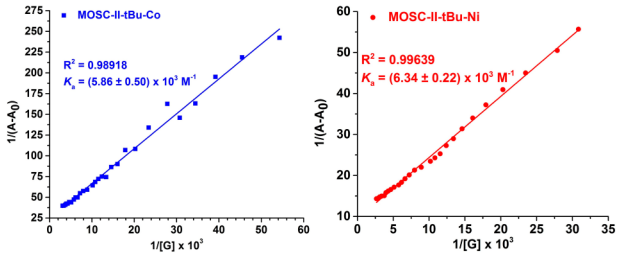

Figure 5. Linear fits of the aspirin titration data to Benesi−Hildebrand equation for MOSC-II-tBu-Co (left) and MOSC-II-tBu-Ni (right).

values are substantially lower than those calculated for the binding of MB with the same MOSCs (Figure 3, right). The stronger binding of MB with the MOSCs compared to aspirin can be partially attributed to its larger conjugation backbone (molecular dimension of MB: 4.0 Å x 7.9 Å x 16.3 Å[102]), which likely leads to a wider host−guest binding surface. The cationic nature of MB may also play an important role in tuning the binding strength with the MOSCs, which are rich in electron-negative oxygen atoms. It should be noted that within experimental uncertainty, the two analogues, MOSC-II-tBu-Co and MOSC-II-tBu-Ni have an essentially identical association constant for the aspirin binding.

While the smaller molecular size of aspirin may in part lead to its weaker binding strength with the MOSCs, it seems to compensate this deficit by achieving a higher binding stoichiometric ratio. A plot of UV−vis absorbance (at 347 nm) vs aspirin equivalent for MOSC-II-tBu-Co reveals a titration profile typically seen in substrate binding to enzymes[100] (Figure 6, left). At low guest equivalents, nearly all aspirin added binds to the MOSC and it follows a linear relation with the absorbance. The tangent at this part of the titration curve thus represents the increase of host−guest complex concentration. At higher aspirin concentrations, only part of the guest binds to the MOSC owing to medium or weak binding strength, causing deviation of the titration curve from

dx.doi.org/10.1021/ja502839b | J. Am. Chem. Soc. 2014, 136, 7480−7491

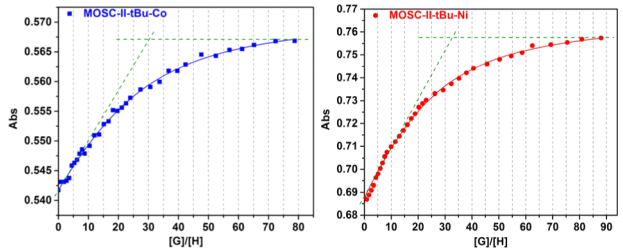

Figure 6. Plots of absorbance vs guest/host molar ratio for the binding of aspirin to MOSC-II-tBu-Co (left) and MOSC-II-tBu-Ni (right), indicating a binding stoichiometric ratio of ∼30 for both MOSCs.

the initial tangent. The UV−vis absorbance continues to increase upon further addition of aspirin until it approaches a saturation plateau, which can be indicated by an asymptotic line. The intersection point of the initial tangent and the asymptote corresponds to a stoichiometric ratio of ∼30 for the binding of aspirin to MOSC-II-tBu-Co. This is a rather remarkable result, as it suggests that binding to the MOSC may provide an effective vehicle to drastically increase local molar concentration of drug molecules, an aspect directly relevant for use of MOSCs in drug delivery applications.[65] It is also noteworthy that a similar plot of UV−vis absorbance (at 348 nm) vs aspirin equivalent reveals a similar aspirin binding stoichiometry (∼33) for the nickel analogue MOSC-II-tBu-Ni (Figure 6, right), confirming that metal ions play a negligible role in the solution guest binding of the MOSCs.

To appreciate how such a large number of aspirin molecules might be included within the MOSC structure, we carried out an analogous aspirin titration study by replacing the MOSCs with either TBSC or the tetranuclear complex.[92] These control experiments show that each sulfonylcalix[4]arene unit in either surrogate host binds to ∼2 aspirin molecules under similar conditions (Figures S24−S27). Therefore, it is plausible that the type II MOSCs encapsulate ∼12 molecules of aspirin through their six *exo* cavities, and entrap the other 18 or so aspirin molecules inside the *endo* cavity. It is possible that, among the 18 or so aspirin molecules residing inside, 12 are directly paring with the 12 BDC units that define the *endo* cavity through face-to-face $\pi-\pi$ interactions, while the remaining 6 or so aggregate at the center of the *endo* cavity.

Solid-State Porosity. Although the solution guest binding of type II MOSCs reveals very little variation among the structural analogues, their solid-state behavior is shown to be much more diverse. For example, the subtle difference in the crystal packing of MOSC-II-tBu-Co and MOSC-II-tBu-Ni is clearly reflected in the solid−liquid adsorption experiments. The hydrolytic stability of MOSCs has allowed the examination of their binding properties in an aqueous environment. When the solids of evacuated MOSC-II-tBu-Co were placed in an aqueous solution containing MB, the MOSC was found to adsorb ca. 5 equiv of the dye, as confirmed by the UV−vis studies (Figure 7; Figure S28). While the solids of evacuated MOSC-II-tBu-Ni also adsorb MB from an aqueous solution, it shows a significantly slower adsorption rate than MOSC-II-tBu-Co under otherwise identical conditions (Figure 7; Figure S29). The adsorption kinetic profiles of both MOSCs are found to fit reasonably well (with the exception of a few initial data points) to the pseudo-second order kinetic model (Figure 8),[91] which indicates a sorbent-dependent sorption mechanism.[103] The linear fit results reveal a similar equilibrium adsorption capacity for both compounds, which reach a MB/MOSC ratio of 5.3−

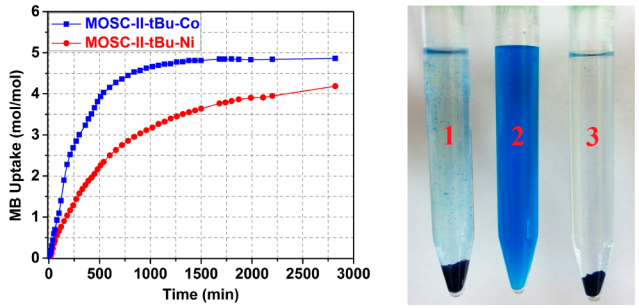

Figure 7. (Left) Methylene blue adsorption kinetic profiles of MOSC-II-tBu-Ni and MOSC-II-tBu-Co at a solid−liquid interface; (right) photographs of methylene blue solutions upon addition of MOSC-II-tBu-Ni (tube no. 1), no MOSC (tube no. 2), and MOSC-II-tBu-Co (tube no. 3).

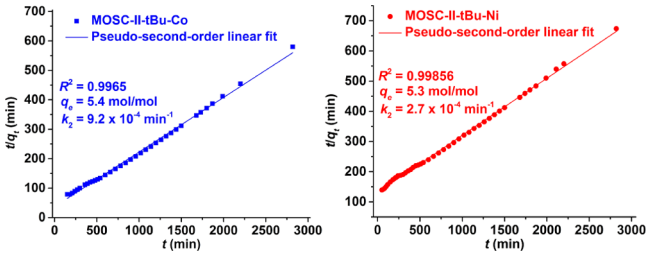

Figure 8. Linear fits of the methylene blue adsorption profiles of MOSC-II-tBu-Co (left) and MOSC-II-tBu-Ni (right) to the pseudo-second-order kinetic rate equation.

5.4 under saturation conditions. It is worth noting that these MB/MOSC stoichiometric ratios are considerably lower than the corresponding values (∼7) determined from the homogeneous solutions (Table S4), suggesting that the MOSC cavities are not fully accessible to guest molecules in the solid state, presumably due to the increased steric hindrance as a result of the solid-state packing. Despite their comparable adsorption capacity, the rate constant of MOSC-II-tBu-Co ($k_2 = 9.2 \times 10^{-4}$ min^{-1}) is more than 3 times that of MOSC-II-tBu-Ni ($k_2 = 2.7 \times 10^{-4}$ min^{-1}). We attribute the faster adsorption kinetics of MOSC-II-tBu-Co to its more open crystal packing (Figure 2), as the larger channels are anticipated to facilitate the transportation of relatively bulky MB molecules.

Interestingly, adsorption analysis at the solid−gas interface (Figure 9; Figure S30) reveals a somewhat unexpected trend. MOSC-II-tBu-Ni is persistently found to have a higher overall gas adsorption capacity than that of MOSC-II-tBu-Co, as indicated by its greater uptake of N_2 and O_2 at 77 K and CO_2 at 196 K. The Brunauer−Emmett−Teller (BET) surface area based on the N_2 adsorption isotherms at 77 K is calculated to

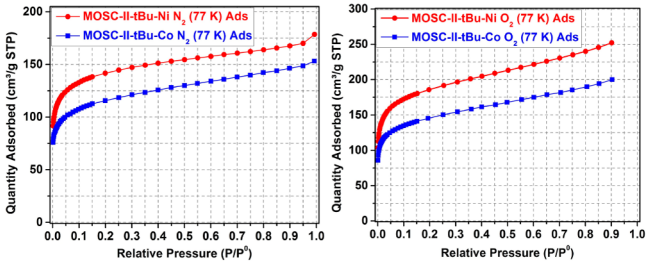

Figure 9. N_2 (left) and O_2 (right) adsorption isotherms (77 K) of MOSC-II-tBu-Ni and MOSC-II-tBu-Co.

dx.doi.org/10.1021/ja502839b | J. Am. Chem. Soc. 2014, 136, 7480−7491

be 523 m^2/g for MOSC-II-tBu-Ni and 423 m^2/g for MOSC-II-tBu-Co, despite the narrower channel size of the nickel compound. Furthermore, the gas adsorption capacity of both MOSC-II-tBu-Ni and MOSC-II-tBu-Co is considerably lower than expected from their respective, largely open crystal structure. As will be elaborated below, these puzzling results can be rationalized by considering the inherent mobility of the MOSC molecules in the solid state, which is essentially sustained by weak van der Waals interactions. In particular, we envision that the solvent removal process required for gas adsorption analysis may have led to a spatial reorganization of the container molecules, which result in a disordering structural character. The structural disordering is evidenced by the poor X-ray powder diffraction patterns of the dried MOSC samples, which exhibit broad and ill-defined peaks (Figure S31). On the other hand, the structure-dependent adsorption properties of the MOSCs at the solid−liquid interface demonstrated above strongly imply that certain elements of their crystal packing have been reasonably well maintained. The proposed solid-state mobility of the MOSC molecules is also in line with the observation made by Atwood and co-workers, who discovered more than a decade ago that molecules of *p-tert*-butylcalix[4]-arene in nonporous solid forms undergo significant positional and/or orientational rearrangement to facilitate guest uptake and release.[104]

The structural flexibility of MOSC-based solids may have also played a key role in dictating the solid−gas adsorption behavior of the MOSC-II-tPen-Ni/Co and MOSC-II-tOc-Ni/Co/Mg series, which crystallize exclusively in the *I*4/*m* space group and are thus iso-structural with MOSC-II-tBu-Co. The seemingly insignificant modification from *tert*-butyl groups to slightly bulkier *tert*-pentyl or *tert*-octyl moieties (Scheme 1) not only impacts the solid-state packing of the MOSCs as detailed previously but also leads to drastically distinct N_2/O_2 adsorption behavior among crystallographically equivalent structures. While the tetragonal MOSC-II-tBu-Co phase adsorbs a considerable amount of N_2 gas at 77 K and 1 atm (~150 cm^3/g STP, Figure 9), the isomorphic analogues MOSC-II-tPen-Ni/Co and MOSC-II-tOc-Ni/Mg/Co all exhibit essentially negligible N_2 uptake under otherwise identical conditions (Figure 10 and Figure S32), indicating an unexpectedly low porosity for these molecular solids. The O_2 adsorption profiles at 77 K follow a similar trend for most of the *tert*-pentyl and *tert*-octyl derivatives, confirming their lack of solid-state porosity. The low-porosity nature of these solid samples is further evidenced by their solid−liquid adsorption profiles, which show little uptake of MB (Figure S33) under conditions comparable to those used for the *tert*-butyl MOSCs (vide supra). Notably, one member of the *tert*-pentyl/*tert*-octyl series, MOSC-II-tPen-Ni, stands out as a remarkable exception, adsorbing a substantial amount of O_2 at 77 K and reaching ca. 110 cm^3/g STP at saturation (Figure 10, top left). This result was reproducible and unlikely caused by factors such as variations in material activation (Figure S34), since all MOSC samples were treated in the exact same manner prior to gas adsorption analysis.

The apparent O_2/N_2 adsorption selectivity demonstrated by MOSC-II-tPen-Ni is particularly intriguing and exemplifies a scenario distinct from the few known examples of O_2-selective metal−organic adsorbents.[105,106] While the O_2 adsorption selectivity of these previously reported materials is accounted for on a chemisorption basis, the lack of any unique O_2 binding sites in MOSC-II-tPen-Ni compared to other members of the

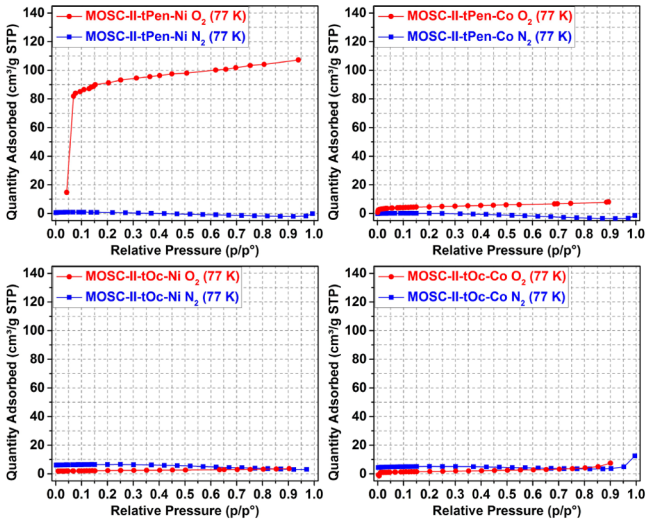

Figure 10. O_2 and N_2 adsorption isotherms (77 K) for MOSC-II-tPen-Ni (top left), MOSC-II-tPen-Co (top right), MOSC-II-tOc-Ni (bottom left), and MOSC-II-tOc-Co (bottom right).

tert-pentyl/*tert*-octyl series suggests that the chemisorption mechanism is not a significant factor. Instead, the O_2/N_2 adsorption selectivity observed in MOSC-II-tPen-Ni is more likely due to a physisorption principle based on the pore dimension of the *evacuated* solid and the subtle difference in the kinetic diameters of N_2 (3.64 Å) and O_2 (3.46 Å).[107] Indeed, the observed O_2/N_2 selectivity can be rationalized by the same argument put forth above, i.e., removal of solvent molecules causes partial structural collapse of the MOSC solids. Specifically, the rearrangement of MOSC-II-tPen-Ni molecules in the solid state as a result of evacuation gives rise to an average pore diameter that lies just between 3.46 and 3.64 Å, thus excluding kinetically larger N_2 molecules while permitting the inclusion of smaller O_2 species.

We postulate that the degree of structural collapse and the resulting average pore dimension directly correlate with the molecular size of the MOSCs (Scheme 3), as does their solid-state packing. As previously discussed, we anticipate the molecular size of type II MOSCs to follow the trend MOSC-II-tBu-Ni < MOSC-II-tBu-Co < MOSC-II-tPen-Ni < MOSC-II-tPen-Co < MOSC-II-tOc-Ni < MOSC-II-tOc-Mg < MOSC-II-tOc-Co. Crystals of MOSC-II-tBu-Ni/Co exhibit relatively less structural rearrangement upon solvent removal because smaller molecules already have a higher packing efficiency in the solid state, leading to a higher level of structural ordering that better retains the initial porous structure. MOSC-II-tBu-Ni/Co thus adsorb both N_2 and O_2 to a considerable degree. The slightly smaller molecular size of MOSC-II-tBu-Ni accounts for its higher gas adsorption capacity than that of MOSC-II-tBu-Co (Figure 9; Figure S30). In contrast, solids of larger MOSC-II-tPen-Co and MOSC-II-tOc-Ni/Mg/Co molecules undergo more pronounced structural collapse upon evacuation in order to achieve a higher packing efficiency and gain further thermodynamic stability, thus affording materials that are essentially nonporous to both N_2 and O_2. The exceptional MOSC-II-tPen-Ni material has an intermediate molecular size and displays transitioning behavior bordering the two scenarios, i.e., its structural collapse operates on such a level that it generates an average pore dimension small enough to exclude N_2 but large enough to accommodate O_2. We emphasize that the proposed theory (Scheme 3) is a speculative

dx.doi.org/10.1021/ja502839b | J. Am. Chem. Soc. 2014, 136, 7480−7491

Scheme 3. A Proposed Mechanism To Account for the N_2/O_2 Adsorption Behavior of Type II MOSCs[a]

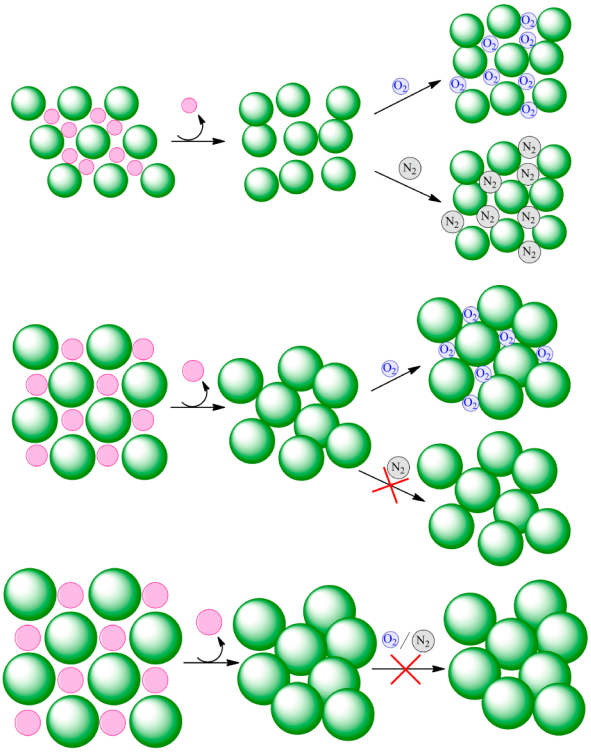

[a]Light-green spheres represent MOSCs of an increasing molecular size, and pink spheres illustrates solvent molecules.

and simplistic model that takes into account the size-selectivity principle only; the actual mechanism may involve additional considerations including a guest-induced "breathing" phenomenon.[108] We are currently examining the hypothesis in greater details using a combined experimental and computational approach and employing the pair distribution function (PDF) method;[109] the result of this ongoing investigation is beyond the scope of the present study and will be communicated in due course.

CONCLUSION

We demonstrate that sulfonylcalixarene-based metal−organic supercontainers are an extremely versatile family of molecular containers, which feature highly tunable structural and functional characteristics. Using type II MOSCs as a model system, we confirm that container molecules may indeed exhibit markedly distinct host−guest chemistry depending on whether the guest-binding event takes place in solution or in solid state. That this phase-specific binding behavior arises is a testimony of the different mechanisms through which the molecular recognition of MOSCs is regulated at different interfaces. In the solution state, the guest binding is primarily determined by the individual MOSC architecture, whereas in the solid state, spatial organization of MOSC molecules also plays a crucial role. The host−guest chemistry of MOSCs in the solid state is of particular interest, as it not only highlights the often much more dynamic nature of molecular solids than generally believed, but also underscores the effectiveness of achieving high adsorption selectivity in porous materials through compromise of adsorption capacity. Our finding thus raises further questions concerning how general this strategy is and whether it can be applied to other classes of molecular solids such as fullerenes or even biomolecules. Addressing these important aspects will have far-reaching impacts on our ability to design materials with task-specific function.

ASSOCIATED CONTENT

Supporting Information

Structural, spectroscopic, and additional characterizations of the new compounds. This material is available free of charge via the Internet at http://pubs.acs.org.

AUTHOR INFORMATION

Corresponding Author

Zhenqiang.Wang@usd.edu

Notes

The authors declare no competing financial interest.

ACKNOWLEDGMENTS

The authors acknowledge the National Science Foundation (CHE-1229035) for the purchase of a Bruker 400 MHz NMR spectrometer. The authors also thank Mr. S. Tamang for assistance in the syntheses of MOSC-II-tBu-Co and MOSC-II-tBu-Ni. This work is supported by the University of South Dakota and South Dakota EPSCoR.

REFERENCES

(1) Worsdorfer, B.; Woycechowsky, K. J.; Hilvert, D. *Science* **2011**, *331*, 589.
(2) Cram, D. J.; Cram, J. M. *Container Molecules and Their Guests*; The Royal Society of Chemistry: Cambridge, England, 1997.
(3) Albrecht, M.; Hahn, F. E.; Ajami, D. *Chemistry of Nanocontainers*; Springer, 2012.
(4) Gibb, C. L. D.; Gibb, B. C. *J. Am. Chem. Soc.* **2004**, *126*, 11408.
(5) Liu, X. J.; Liu, Y.; Li, G.; Warmuth, R. *Angew. Chem., Int. Ed.* **2006**, *45*, 901.
(6) Liu, Y.; Liu, X.; Warmuth, R. *Chem.—Eur. J.* **2007**, *13*, 8953.
(7) Ferrand, Y.; Crump, M. P.; Davis, A. P. *Science* **2007**, *318*, 619.
(8) Holst, J. R.; Trewin, A.; Cooper, A. I. *Nat. Chem.* **2010**, *2*, 915.
(9) Mastalerz, M.; Schneider, M. W.; Oppel, I. M.; Presly, O. *Angew. Chem., Int. Ed.* **2011**, *50*, 1046.
(10) Kang, S. O.; Llinares, J. M.; Day, V. W.; Bowman-James, K. *Chem. Soc. Rev.* **2010**, *39*, 3980.
(11) Icli, B.; Christinat, N.; Tonnemann, J.; Schuttler, C.; Scopelliti, R.; Severin, K. *J. Am. Chem. Soc.* **2009**, *131*, 3154.
(12) Nishiyabu, R.; Kubo, Y.; James, T. D.; Fossey, J. S. *Chem. Commun.* **2011**, *47*, 1124.
(13) Avellaneda, A.; Valente, P.; Burgun, A.; Evans, J. D.; Markwell-Heys, A. W.; Rankine, D.; Nielsen, D. J.; Hill, M. R.; Sumby, C. J.; Doonan, C. J. *Angew. Chem., Int. Ed.* **2013**, *52*, 3746.
(14) Saalfrank, R. W.; Stark, A.; Peters, K.; von Schnering, H. G. *Angew. Chem., Int. Ed. Engl.* **1988**, *27*, 851.
(15) Fujita, M.; Oguro, D.; Miyazawa, M.; Oka, H.; Yamaguchi, K.; Ogura, K. *Nature* **1995**, *378*, 469.
(16) Yoshizawa, M.; Klosterman, J. K.; Fujita, M. *Angew. Chem., Int. Ed.* **2009**, *48*, 3418.
(17) Caulder, D. L.; Powers, R. E.; Parac, T. N.; Raymond, K. N. *Angew. Chem., Int. Ed.* **1998**, *37*, 1840.
(18) Caulder, D. L.; Raymond, K. N. *Acc. Chem. Res.* **1999**, *32*, 975.
(19) Olenyuk, B.; Whiteford, J. A.; Fechtenkötter, A.; Stang, P. J. *Nature* **1999**, *398*, 796.
(20) Chakrabarty, R.; Mukherjee, P. S.; Stang, P. J. *Chem. Rev.* **2011**, *111*, 6810.
(21) McKinlay, R. M.; Cave, G. W. V.; Atwood, J. L. *Proc. Natl. Acad. Sci. U.S.A.* **2005**, *102*, 5944.
(22) Dalgarno, S. J.; Power, N. P.; Atwood, J. L. *Coord. Chem. Rev.* **2008**, *252*, 825.

(23) Moulton, B.; Lu, J. J.; Mondal, A.; Zaworotko, M. J. *Chem. Commun.* **2001**, 863.
(24) Eddaoudi, M.; Kim, J.; Wachter, J. B.; Chae, H. K.; O'Keeffe, M.; Yaghi, O. M. *J. Am. Chem. Soc.* **2001**, *123*, 4368.
(25) Tranchemontagne, D. J.; Ni, Z.; O'Keeffe, M.; Yaghi, O. M. *Angew. Chem., Int. Ed.* **2008**, *47*, 5136.
(26) Mal, P.; Breiner, B.; Rissanen, K.; Nitschke, J. R. *Science* **2009**, *324*, 1697.
(27) Farrell, J. R.; Mirkin, C. A.; Guzei, I. A.; Liable-Sands, L. M.; Rheingold, A. L. *Angew. Chem., Int. Ed. Engl.* **1998**, *37*, 465.
(28) Clever, G. H.; Tashiro, S.; Shionoya, M. *Angew. Chem., Int. Ed.* **2009**, *48*, 7010.
(29) Ward, M. D. *Chem. Commun.* **2009**, 4487.
(30) Mirtschin, S.; Slabon-Turski, A.; Scopelliti, R.; Velders, A. H.; Severin, K. *J. Am. Chem. Soc.* **2010**, *132*, 14004.
(31) Li, J. R.; Zhou, H. C. *Nat. Chem.* **2010**, *2*, 893.
(32) Liu, M.; Liao, W. P.; Hu, C. H.; Du, S. C.; Zhang, H. J. *Angew. Chem., Int. Ed.* **2012**, *51*, 1585.
(33) Amouri, H.; Desmarets, C.; Moussa, J. *Chem. Rev.* **2012**, *112*, 2015.
(34) Young, N. J.; Hay, B. P. *Chem. Commun.* **2013**, *49*, 1354.
(35) Wyler, R.; Demendoza, J.; Rebek, J. *Angew. Chem., Int. Ed. Engl.* **1993**, *32*, 1699.
(36) Hof, F.; Craig, S. L.; Nuckolls, C.; Rebek, J. *Angew. Chem., Int. Ed.* **2002**, *41*, 1488.
(37) Conn, M. M.; Rebek, J. *Chem. Rev.* **1997**, *97*, 1647.
(38) MacGillivray, L. R.; Atwood, J. L. *Nature* **1997**, *389*, 469.
(39) Atwood, J. L.; Barbour, L. J.; Jerga, A. *Proc. Natl. Acad. Sci. U.S.A.* **2002**, *99*, 4837.
(40) Liu, Y. Z.; Hu, C. H.; Comotti, A.; Ward, M. D. *Science* **2011**, *333*, 436.
(41) Cavarzan, A.; Scarso, A.; Sgarbossa, P.; Strukul, G.; Reek, J. N. H. *J. Am. Chem. Soc.* **2011**, *133*, 2848.
(42) Adriaenssens, L.; Ballester, P. *Chem. Soc. Rev.* **2013**, *42*, 3261.
(43) (a) Stang, P. J.; Olenyuk, B. *Acc. Chem. Res.* **1997**, *30*, 502. (b) Leininger, S.; Olenyuk, B.; Stang, P. J. *Chem. Rev.* **2000**, *100*, 853. (c) Seidel, S. R.; Stang, P. J. *Acc. Chem. Res.* **2002**, *35*, 972. (d) Stang, P. J. *J. Am. Chem. Soc.* **2012**, *134*, 11829. (e) Cook, T. R.; Zheng, Y. R.; Stang, P. J. *Chem. Rev.* **2013**, *113*, 734.
(44) Sudik, A. C.; Millward, A. R.; Ockwig, N. W.; Côte, A. P.; Kim, J.; Yaghi, O. M. *J. Am. Chem. Soc.* **2005**, *127*, 7110.
(45) Duriska, M. B.; Neville, S. M.; Lu, J. Z.; Iremonger, S. S.; Boas, J. F.; Kepert, C. J.; Batten, S. R. *Angew. Chem., Int. Ed.* **2009**, *48*, 8919.
(46) Li, J. R.; Zhou, H. C. *Angew. Chem., Int. Ed.* **2009**, *48*, 8465.
(47) Zhao, D.; Yuan, D. Q.; Krishna, R.; van Baten, J. M.; Zhou, H. C. *Chem. Commun.* **2010**, *46*, 7352.
(48) Liu, T. F.; Liu, Y.; Xuan, W. M.; Cui, Y. *Angew. Chem., Int. Ed.* **2010**, *49*, 4121.
(49) Ousaka, N.; Clegg, J. K.; Nitschke, J. R. *Angew. Chem., Int. Ed.* **2012**, *51*, 1464.
(50) Custelcean, R.; Bosano, J.; Bonnesen, P. V.; Kertesz, V.; Hay, B. P. *Angew. Chem., Int. Ed.* **2009**, *48*, 4025.
(51) Custelcean, R.; Bonnesen, P. V.; Duncan, N. C.; Zhang, X. H.; Watson, L. A.; Van Berkel, G.; Parson, W. B.; Hay, B. P. *J. Am. Chem. Soc.* **2012**, *134*, 8525.
(52) Hristova, Y. R.; Smulders, M. M. J.; Clegg, J. K.; Breiner, B.; Nitschke, J. R. *Chem. Sci.* **2011**, *2*, 638.
(53) Freye, S.; Hey, J.; Torras-Galan, A.; Stalke, D.; Herbst-Irmer, R.; John, M.; Clever, G. H. *Angew. Chem., Int. Ed.* **2012**, *51*, 2191.
(54) Liu, Y.; Wu, X.; He, C.; Jiao, Y.; Duan, C. Y. *Chem. Commun.* **2009**, 7554.
(55) Jiao, Y.; Zhang, J.; Zhang, L. J.; Lin, Z. H.; He, C.; Duan, C. Y. *Chem. Commun.* **2012**, *48*, 6022.
(56) Ito, H.; Kusukawa, T.; Fujita, M. *Chem. Lett.* **2000**, 598.
(57) Yoshizawa, M.; Tamura, M.; Fujita, M. *Science* **2006**, *312*, 251.
(58) Fiedler, D.; Bergman, R. G.; Raymond, K. N. *Angew. Chem., Int. Ed.* **2004**, *43*, 6748.
(59) Pluth, M. D.; Bergman, R. G.; Raymond, K. N. *Science* **2007**, *316*, 85.
(60) Koblenz, T. S.; Wassenaar, J.; Reek, J. N. H. *Chem. Soc. Rev.* **2008**, *37*, 247.
(61) Breiner, B.; Clegg, J. K.; Nitschke, J. R. *Chem. Sci.* **2011**, *2*, 51.
(62) Smulders, M. M. J.; Nitschke, J. R. *Chem. Sci.* **2012**, *3*, 785.
(63) Huang, S. L.; Lin, Y. J.; Hor, T. S. A.; Jin, G. X. *J. Am. Chem. Soc.* **2013**, *135*, 8125.
(64) Zhao, D.; Tan, S. W.; Yuan, D. Q.; Lu, W. G.; Rezenom, Y. H.; Jiang, H. L.; Wang, L. Q.; Zhou, H. C. *Adv. Mater.* **2011**, *23*, 90.
(65) Therrien, B. *Top. Curr. Chem.* **2012**, *319*, 35.
(66) Lewis, J. E. M.; Gavey, E. L.; Cameron, S. A.; Crowley, J. D. *Chem. Sci.* **2012**, *3*, 778.
(67) Zhou, H. C.; Long, J. R.; Yaghi, O. M. *Chem. Rev.* **2012**, *112*, 673.
(68) McKeown, N. B. *J. Mater. Chem.* **2010**, *20*, 10588.
(69) Mastalerz, M. *Angew. Chem., Int. Ed.* **2010**, *49*, 5042.
(70) Tian, J.; Thallapally, P. K.; McGrail, B. P. *CrystEngComm* **2012**, *14*, 1909.
(71) Smulders, M. M. J.; Zarra, S.; Nitschke, J. R. *J. Am. Chem. Soc.* **2013**, *135*, 7039.
(72) Tozawa, T.; Jones, J. T. A.; Swamy, S. I.; Jiang, S.; Adams, D. J.; Shakespeare, S.; Clowes, R.; Bradshaw, D.; Hasell, T.; Chong, S. Y.; Tang, C.; Thompson, S.; Parker, J.; Trewin, A.; Bacsa, J.; Slawin, A. M. Z.; Steiner, A.; Cooper, A. I. *Nat. Mater.* **2009**, *8*, 973.
(73) Inokuma, Y.; Arai, T.; Fujita, M. *Nat. Chem.* **2010**, *2*, 780.
(74) Inokuma, Y.; Kawano, M.; Fujita, M. *Nat. Chem.* **2011**, *3*, 349.
(75) Ning, G.-H.; Inokuma, Y.; Fujita, M. *Chem.—Asian J.* **2013**, *8*, 2596.
(76) Mitra, T.; Jelfs, K. E.; Schmidtmann, M.; Ahmed, A.; Chong, S. Y.; Adams, D. J.; Cooper, A. I. *Nat. Chem.* **2013**, *5*, 276.
(77) Bojdys, M. J.; Briggs, M. E.; Jones, J. T. A.; Adams, D. J.; Chong, S. Y.; Schmidtmann, M.; Cooper, A. I. *J. Am. Chem. Soc.* **2011**, *133*, 16566.
(78) Harris, K.; Sun, Q.-F.; Sato, S.; Fujita, M. *J. Am. Chem. Soc.* **2013**, *135*, 12497.
(79) Jones, J. T. A.; Hasell, T.; Wu, X. F.; Bacsa, J.; Jelfs, K. E.; Schmidtmann, M.; Chong, S. Y.; Adams, D. J.; Trewin, A.; Schiffman, F.; Cora, F.; Slater, B.; Steiner, A.; Day, G. M.; Cooper, A. I. *Nature* **2011**, *474*, 367.
(80) Kumagai, H.; Hasegawa, M.; Miyanari, S.; Sugawa, Y.; Sato, Y.; Hori, T.; Ueda, S.; Kamiyama, H.; Miyano, S. *Tetrahedron Lett.* **1997**, *38*, 3971.
(81) Morohashi, N.; Narumi, F.; Iki, N.; Hattori, T.; Miyano, S. *Chem. Rev.* **2006**, *106*, 5291.
(82) Iki, N.; Kumagai, H.; Morohashi, N.; Ejima, K.; Hasegawa, M.; Miyanari, S.; Miyano, S. *Tetrahedron Lett.* **1998**, *39*, 7559.
(83) Dai, F.-R.; Wang, Z. *J. Am. Chem. Soc.* **2012**, *134*, 8002.
(84) Gutsche, C. D. *Calixarenes: An Introduction*; 2nd ed.; The Royal Society of Chemistry: Cambridge, U.K., 2008.
(85) Atwood, J. L.; Barbour, L. J.; Dalgarno, S. J.; Hardie, M. J.; Raston, C. L.; Webb, H. R. *J. Am. Chem. Soc.* **2004**, *126*, 13170.
(86) Xiong, K.; Jiang, F.; Gai, Y.; Yuan, D.; Chen, L.; Wu, M.; Su, K.; Hong, M. *Chem. Sci.* **2012**, *3*, 2321.
(87) Morohashi, N.; Iki, N.; Sugawara, A.; Miyano, S. *Tetrahedron* **2001**, *57*, 5557.
(88) Iki, N.; Kabuto, C.; Fukushima, T.; Kumagai, H.; Takeya, H.; Miyanari, S.; Miyashi, T.; Miyano, S. *Tetrahedron* **2000**, *56*, 1437.
(89) Schalley, C. A. *Analytical Methods in Supramolecular Chemistry*; Wiley: Weinheim, Germany, 2012.
(90) Benesi, H. A.; Hildebrand, J. *J. Am. Chem. Soc.* **1949**, *71*, 2703.
(91) Ho, Y. S.; McKay, G. *Trans. Inst. Chem. Eng.* **1998**, *76*, 332.
(92) Kajiwara, T.; Kobashi, T.; Shinagawa, R.; Ito, T.; Takaishi, S.; Yamashita, M.; Iki, N. *Eur. J. Inorg. Chem.* **2006**, 1765.
(93) Braun, M. E.; Steffek, C. D.; Kim, J.; Rasmussen, P. G.; Yaghi, O. M. *Chem. Commun.* **2001**, 2532.
(94) Shannon, R. *Acta Crystallogr.* **1976**, *A32*, 751.
(95) Gassensmith, J. J.; Arunkumar, E.; Smith, B. D. In *Molecular Encapsulation*; John Wiley & Sons: Chichester, 2010; p 309.

(96) Kumar, A.; Mansour, H. M.; Friedman, A.; Blough, E. R. *Nanomedicine in Drug Delivery*; CRC Press Taylor & Francis: Boca Raton, FL, 2013.
(97) Houk, K. N.; Leach, A. G.; Kim, S. P.; Zhang, X. Y. *Angew. Chem., Int. Ed.* **2003**, *42*, 4872.
(98) Job, P. *Ann. Chim. (Paris) (Serie 10)* **1928**, *9*, 113.
(99) Hill, Z. D.; MacCarthy, P. *J. Chem. Educ.* **1986**, *63*, 162.
(100) Bisswanger, H. *Enzyme Kinetics: Principles and Methods*, 2*nd Ed.*; Wiley, 2008.
(101) Dai, F.-R.; Becht, D. C.; Wang, Z. *Chem. Commun.* **2014**, *50*, 5385.
(102) Zhao, X.; Bu, X. H.; Wu, T.; Zheng, S. T.; Wang, L.; Feng, P. Y. *Nat. Commun.* **2013**, *4*, 2344.
(103) Ho, Y. S. *Adsorption* **2004**, *10*, 151.
(104) Atwood, J. L.; Barbour, L. J.; Jerga, A.; Schottel, B. L. *Science* **2002**, *298*, 1000.
(105) Murray, L. J.; Dinca, M.; Yano, J.; Chavan, S.; Bordiga, S.; Brown, C. M.; Long, J. R. *J. Am. Chem. Soc.* **2010**, *132*, 7856.
(106) Southon, P. D.; Price, D. J.; Nielsen, P. K.; McKenzie, C. J.; Kepert, C. J. *J. Am. Chem. Soc.* **2011**, *133*, 10885.
(107) Yang, R. T. *Adsorbents: Fundamentals and Applications*; John Wiley & Sons, Inc.: Hoboken, NJ, 2003.
(108) Férey, G.; Serre, C. *Chem. Soc. Rev.* **2009**, *38*, 1380.
(109) Chapman, K. W.; Sava, D. F.; Halder, G. J.; Chupas, P. J.; Nenoff, T. M. *J. Am. Chem. Soc.* **2011**, *133*, 18583.